Vibrational Spectroscopy xxx (2012) xxx–xxx

Contents lists available at SciVerse ScienceDirect

Vibrational Spectroscopy

journal homepage: www.elsevier.com/locate/vibspec

Quantitative surface plasmon spectroscopy: Determination of the infrared optical constants of living cells

Alexander Zilbershtein[a,*], Michael Golosovsky[a], Vladislav Lirtsman[a], Benjamin Aroeti[b], Dan Davidov[a]

[a] The Racah Institute of Physics, The Hebrew University of Jerusalem, Jerusalem, Israel
[b] Department of Cell and Development Biology, The Alexander Silberman Institute of Life Sciences, The Hebrew University of Jerusalem, Jerusalem, Israel

ARTICLE INFO

Article history:
Received 6 July 2011
Received in revised form 23 January 2012
Accepted 25 January 2012
Available online xxx

Keywords:
FT-IR spectroscopy
Surface plasmon resonance
Optical constants
Living cells spectroscopy

ABSTRACT

Fourier transform infrared (FTIR) spectroscopy gives a great amount of information on the distribution of chemical components in biological objects, in particular cells, in a label-free manner. We report on the development of the spectroscopic technique that combines the surface plasmon resonance (SPR) and the FTIR. Our method is based on the original processing of SPR measurements at varying angles and wavelengths and yields the complex refractive index of the analyte in a broad wavelength region. Contrary to previous SPR studies which yielded information about refractive index variation only, our technique gives absolute optical constants of the examined medium. Using this approach, we studied living Madin Darby canine kidney (MDCK) epithelial cells cultured in their natural aqueous environment and measured their optical constants. We showed that our technique has the ability to distinguish absorption lines of certain chemical components of the cells, such as the absorption lines of a CH_n bonds which are characteristic mostly for cell membrane lipids.

1. Introduction

Infrared spectroscopy is a powerful tool that is used for analyzing biological specimens. It is commonly applied for sensing and imaging of the distribution of chemical components in cells in a label-free manner [1]. Fourier transform infrared (FTIR) spectroscopy provides molecular specificity by measuring the intensity of specific absorption lines, which can be correlated to biological processes in cells. FTIR studies of cell monolayers [2], single cells [3,4] and cellular components [5] were performed. The medical and pharmacological applications induced studies of infrared spectroscopic signatures associated with cell cycle and cell death [6–8], disease-associated molecular changes [9–12], and cell and tissue response to drugs [13–15]. However, FTIR spectroscopic studies of living cells in aqueous environments are hampered by the strong water absorption in the mid-infrared region. Although this complication can be circumvented by using the synchrotron source for data acquisition [3,4,6], the most part of the FTIR spectroscopic studies of cell cultures have been performed on dried or fixed samples whereby dynamic processes, such as cell death or drug uptake, were studied by drying or fixing cultured cells at various stages of biological activities. However, the drying or fixation might lead to structural changes in cells [16], and also prevent measuring of the dynamic processes in real time. That is why it is highly desirable to study live cell cultures with FTIR spectroscopy in an appropriate tissue culture medium in order to detect in real time the cells' response to environmental changes (temperature, bacteria or virus effects, drugs insertion, etc.).

The infrared surface plasmon resonance (SPR) technique is a good candidate for this task [17–22]. Unlike conventional FTIR spectroscopy, the surface plasmon wave probes only a thin layer of dielectric material (analyte) positioned on top of the metal-coated substrate. That is why the water absorption does not saturate the signal received by the detector to the extent as it does in transmission measurements, thus allowing the spectroscopy in vivo with reasonable signal-to-noise ratio. In addition, the FTIR-SPR method is particularly advantageous for biosensing, because it is a label-free technique that can monitor the kinetics of biological processes in real time [17]. In comparison to FTIR-ATR (attenuated total reflection) [7,11,15] that also probes a thin layer, the SPR in general has a superior sensitivity due to its resonant character [23,24]. While the penetration depth of the ATR spectroscopy varies from 0.3 μm at 5000 cm^{-1} up to 1.2 μm at 2500 cm^{-1} (for ZnSe prism), in such a way that only a small part of the cell is probed, the penetration depth of the FTIR-SPR technique varies from 1 μm at 5000 cm^{-1} up to 5 μm at 2500 cm^{-1} that allows probing the majority of the cell volume, e.g. cell membrane, nuclear, different organelles, and cytoplasm [17].

We report on the development of the FTIR-SPR technique for spectroscopic studies. Conventional SPR studies measure variations

* Corresponding author.
E-mail address: alexander.zilbershtein@mail.huji.ac.il (A. Zilbershtein).

0924-2031/$ – see front matter © 2012 Elsevier B.V. All rights reserved.
doi:10.1016/j.vibspec.2012.01.019

in real part of the refractive index only [17–25], while our FTIR-SPR technique determines the absolute complex refractive index of the examined medium (in particular live cells in aqueous environment) in the broad wavelength region. This technique is based on the modeling of SPR measurements, which takes into account any possible experimental uncertainties, such as: (a) incident beam divergence and beam misalignment; (b) partial polarization of the incident beam; (c) finite extinction ratio of the polarizer; (d) deviation of the optical properties of thin gold film from those of bulk gold; (e) correction to nominal gold film thickness. Using this technique, we studied live Madin Darby canine kidney (MDCK) epithelial cells and measured optical constants of the cells in the 2400–10,000 cm^{-1} spectral region with high precision. We found that the real part of the refractive index of cells, n_{cell}, exceeds that of the water by ~0.03 in the studied spectral region. The imaginary part of the cell refractive index, κ_{cell}, is mainly defined by absorption in the region below 4000 cm^{-1}, and by scattering above 4000 cm^{-1}.

2. Surface plasmon spectroscopy – theoretical background

A surface plasmon (SP) is an electromagnetic surface wave propagating at the metal–dielectric interface whose wave vector is $k_{sp} = k_0\sqrt{\varepsilon_m\varepsilon_d/(\varepsilon_m+\varepsilon_d)}$ [26]. Here k_0 is the wave vector of the incident light, ε_m and ε_d are dielectric permittivities of the metal and dielectric, correspondingly. The electromagnetic field of the SP wave is confined at the metal–dielectric interface and decreases exponentially into both media. Since the field is localized at the interface, the propagation constant of the SP wave is extremely sensitive to tiny changes in complex refractive index of the dielectric, $n_d + i\kappa_d = \varepsilon_d^{1/2}$, in the vicinity of the interface.

The surface plasmon is usually excited using a high refractive index prism with a metal-coated base which is in contact with the dielectric under study (see Fig. 1). The resonant condition for the SP excitation is fulfilled when the projection of the incident light wave vector on the interface, $k_x = n_{pr}k_0\sin\theta_{sp}$, equals the real part of the SP wave vector, k'_{sp}. Here n_{pr} is the refractive index of the prism, and θ_{sp} is the incident angle at the prism–gold interface (Fig. 1). It results in a sharp reflectivity minimum, and at the resonance the following expression holds true [17,26]:

$$n_d(\nu_{min}) = n_{pr}\sin\theta_{sp}\left(\frac{\varepsilon'_m}{\varepsilon'_m - n_{pr}^2\sin^2\theta_{sp}}\right)^{1/2} \quad (1)$$

where $\nu = 1/\lambda$ is the wave number. This equation yields the refractive index of the analyte at a certain wave number which is encoded by the incident angle. By varying the incident angle we force the SP reflectivity minimum to appear at different wave numbers. This gives the possibility to find the refractive index of the analyte in the broad spectral region.

The lossy part of the complex refractive index of the analyte can be found from the analysis of reflectivity. Indeed, the value of the SPR reflectivity minimum is related to the imaginary part of the SP wave vector, k''_{sp}, which is determined by intrinsic losses ε''_m and ε''_d through [17,25]:

$$k''_{sp} = k_0\left(\frac{\varepsilon'_m\varepsilon'_d}{\varepsilon'_m+\varepsilon'_d}\right)^{3/2}\left(\frac{\varepsilon''_d}{\varepsilon'^2_d}+\frac{\varepsilon''_m}{\varepsilon'^2_m}\right) \quad (2)$$

In summary, by measuring the resonant angle of the SPR, we determine the k'_{sp} which yields the refractive index of the dielectric layer at the resonant wave number (Eq. (1)). On the other hand, the reflectivity at resonance yields k''_{sp}, and thus provides information about the imaginary part of dielectric permittivity of the analyte, ε''_d (Eq. (2)).

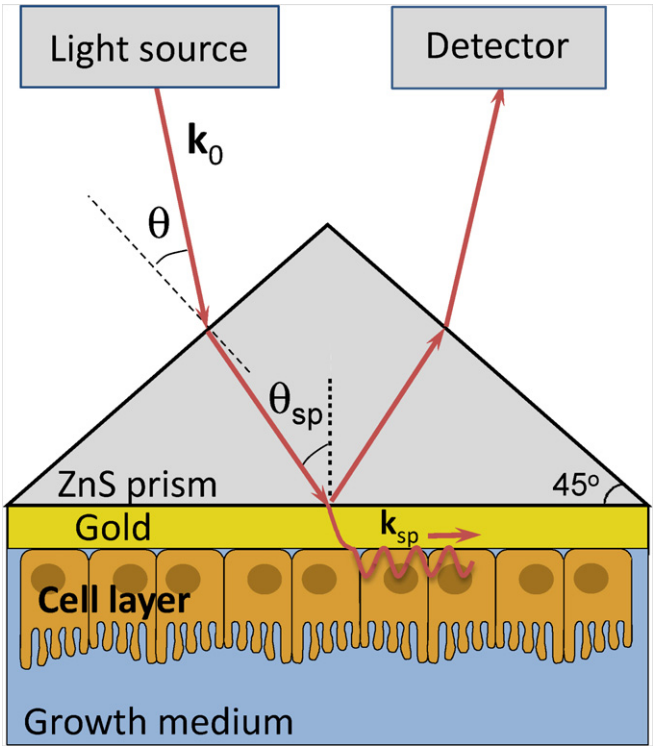

Fig. 1. Surface plasmon excitation using Kretschmann's geometry based on a high refractive index prism coated by the 12–20 nm thick gold film. k_0 is the wave vectors in free space. k_{sp} is the surface plasmon wave vector. θ is the angle between the incident beam and a normal to the prism side. θ_{sp} is the angle of incidence at the prism/gold/dielectric interface. The cell layer is grown directly on gold, and is immersed in growth medium.

The surface plasmon wave probes the refractive index of a thin layer of analyte in the vicinity to the metal, whose thickness is [17,25]

$$\delta_z = I_m\left[\frac{(\varepsilon_m+\varepsilon_d)^{1/2}}{2k_0\varepsilon_d}\right] \quad (3)$$

Biological objects, such as cell layers and cells itself, are spatially inhomogeneous on a micrometer scale in terms of physical morphology and chemical content. For an inhomogeneous medium whose properties vary in the z-direction (perpendicular to the metal–dielectric interface), the SP wave samples the effective refractive index of the analyte, n_{eff}, which is defined as [17]:

$$n_{eff} = \frac{1}{\delta_z}\int_0^\infty n(z)\exp\left(-\frac{z}{\delta_z}\right)dz \quad (4)$$

In this work we utilize SPR measurements at varying angles and wavelengths in order to determine the complex refractive index of the analyte in a broad wavelength region.

3. Materials and methods

3.1. Experimental design – FTIR SPR set up

Our experimental setup is shown in Fig. 2 and it was described in more detail in [18,19,22]. It is based on the right-angle ZnS prism coated with 12–20 nm thick gold film, which was e-beam evaporated on the cleaned prism surface. The prism is attached to the temperature-stabilized flow chamber of 1 ml in volume. The analyte is inserted into the flow chamber by a motorized bee syringe pump equipped with a variable speed controller. The prism–flow chamber assembly is mounted on the goniometric $\theta - 2\theta$ rotating

Please cite this article in press as: A. Zilbershtein, et al., Quantitative surface plasmon spectroscopy: Determination of the infrared optical constants of living cells, Vib. Spectrosc. (2012), doi:10.1016/j.vibspec.2012.01.019

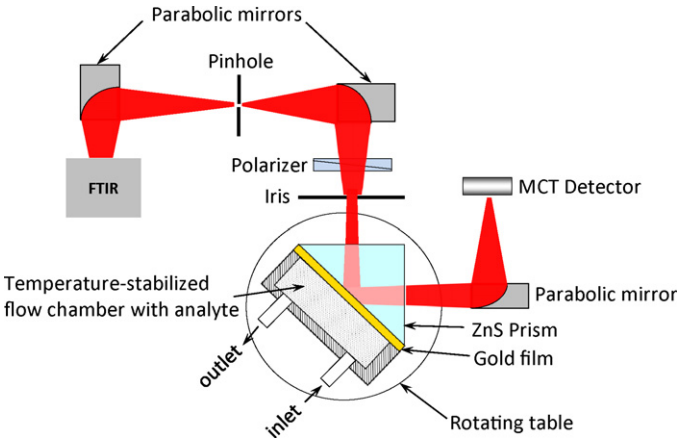

Fig. 2. Experimental FTIR-SPR setup. The polarized beam from the FTIR source is incident on the right angle ZnS prism coated by gold film in contact with the analyte. The reflectivity is measured by the MCT detector coupled to detecting system of the FTIR spectrometer. The measurements at varying angle/wavelength are possible.

stage. The surface plasmon is excited in the Kretschmann's geometry (see Fig. 1) using the Bruker Equinox-55 FTIR spectrometer as the broadband infrared source. Namely, the infrared beam from the external port of the FTIR is collimated and polarized, reflected from the prism and focused onto a liquid-nitrogen-cooled MCT (HgCdTe) detector. The diameter of the beam spot is 3 mm.

3.2. Cell culture preparation for SPR measurements

MDCK cells were routinely cultured on a 10-cm diameter dish in growth medium: minimal essential medium (MEM, Biological Industries, Beit Haemek, Israel), supplemented with 5% fetal calf serum (FCS) and 1% antibiotics (Biological Industries). Cells were maintained in a CO_2 incubator (5% CO_2, 37 °C, 90% humidity). Upon reaching confluence, the cells were washed twice with PBS and detached from the dish by trypsinization (0.25% trypsin/EDTA in Puck's saline A; Biological industries). The cells were then suspended in 10 ml of growth medium, and seeded on top of the Au-coated ZnS prism mounted in the polycarbonate holder, as previously described [21]. Cells were allowed to attach to the gold for at least 3 h in the CO_2 incubator. Thereafter, we added 5 ml of growth medium and the prism was placed in a CO_2 incubator for another 2 days until a uniform cell monolayer was obtained [21].

3.3. SPR measurements with Madin Darby canine kidney (MDCK) living cells

The prism with cells was attached to the flow chamber mounted on a goniometer (Fig. 2), in such a way that the cells on the gold-coated surface faced the flow chamber's volume. The flow chamber was filled with modified Eagle's medium (MEM) Hanks' salts supplemented with 20 mM Hepes, pH 7.5 (MEM-Hepes). The temperature in the flow chamber was kept at 37 °C. The medium was passed through the chamber at a constant flow rate (5 μL/min) during the measurements. We performed SPR measurements at varying incident angle, θ, from 0° up to 31° with a step of 0.25°. The cells were then detached from the gold substrate by trypsin treatment and washed out from the flow chamber. The flow chamber was filled with distilled water at 37 °C, and the SPR measurements were performed once again in order to find the dielectric permittivity of the gold film used in this experiment. In order to check the repeatability of the results we performed three series of measurements with different prisms and cell layers obtained from the same cell culture.

4. Measurement protocol and data processing

4.1. FTIR spectra acquisition

At each incident angle, θ, we measured the reflectivity spectrum for s- and p-polarizations of the incident light, I_p and I_s, and determined their ratio:

$$\rho_m(\nu,\theta) = \frac{I_p(\nu,\theta)}{I_s(\nu,\theta)} \quad (5)$$

In order to compare our experimental data with model predictions we recalculated the measured spectrum, ρ_m, by taking into account: (a) partial polarization of the incident beam, $A(\nu)$, and (b) finite extinction ratio of the polarizer, $E(\nu)$. The partial polarization of the incident beam was found using two polarizers in tandem. The extinction ratio of the polarizer was found using two polarizers in cross-orientation. The reassembled SPR experimental spectrum, $F_{exp}(\nu,\theta)$, has the following form:

$$F_{exp}(\nu,\theta) = \frac{1}{A}\cdot\frac{\rho_m - E}{1 - E\cdot\rho_m} \quad (6)$$

4.2. Optical model

In the next step, we compared the recalculated measured spectrum, F_{exp} (Eq. (6)), with the calculated one, F_{model} [27,28]. The latter takes into account partial transmission at the entrance and exit faces of the prism, T_1 and T_2, the reflectivity at the prism/gold/analyte interface, R, and beam divergence, $L(\theta)$. The optical model yields the ratio of reflectivities for p- and s-polarizations:

$$F_{model}(\nu,\theta) = \int \left(\frac{T_{1p}}{T_{1s}}\right)\left(\frac{R_p}{R_s}\right)\left(\frac{T_{2p}}{T_{2s}}\right) L(\theta)d\theta \quad (7)$$

The reflectivity, R, for both polarizations is given by the Fresnel formula

$$R = \left|\frac{r_{12} + r_{23}\cdot\exp(2ik_{z2}d)}{1 + r_{12}\cdot r_{23}\cdot\exp(2ik_{z2}d)}\right|^2,$$

where $r_{nm} = ((k_{zn}/\varepsilon_n^\alpha) - (k_{zm}/\varepsilon_m^\alpha))/((k_{zn}/\varepsilon_n^\alpha) + (k_{zm}/\varepsilon_m^\alpha))$ is the reflectivity from the infinite thick interface; n and m are numbers that correspond to the 1-prism, 2-gold, 3-analyte; d is the gold film thickness; k_z is the z-component of the wave vector, and $\alpha = 1(0)$ for p(s)-polarized light, correspondingly. The transmission coefficient through the air–prism interface is expressed as: $T_1 = (4k_{air}/n_{pr}^{2\alpha})/(k_{air} + (k_{pr}/n_{pr}^{2\alpha}))^2$, $k_{air} = k_0\cdot\cos\theta$, and $k_{pr} = k_0\sqrt{n_{pr}^2 - \sin^2\theta}$, where n_{pr} is the refractive index of the ZnS prism, taken from [29]. The transmission coefficient through the prism-air interface, T_2, is given by a similar expression where k_{air} is replaced by k_{pr} in the numerator. The factor $L(\theta)$ denotes the incident beam shape and given by a Lorentzian $L(\theta) = (1/\pi)\cdot(\gamma/((\theta-\theta_0)^2 + \gamma^2))$, where $\gamma = 0.26°$ is measured a beam divergence.

In summary, our model allows to find the complex dielectric permittivity of the analyte ε_d from the SPR spectra. To do that, one must know the exact dielectric permittivity of the gold film since this is not universal and depends on film thickness and on evaporation conditions [25,30–33].

4.3. Complex dielectric permittivity of the gold film

In principle, the dielectric permittivity of a gold film could be determined from the SPR reflectivity spectra from the prism/gold/dielectric interface with any dielectric whose optical constants are known. We chose water since its complex refractive index is well-known [34]. The reflectivity from the ZnS/Au/water

Please cite this article in press as: A. Zilbershtein, et al., Quantitative surface plasmon spectroscopy: Determination of the infrared optical constants of living cells, Vib. Spectrosc. (2012), doi:10.1016/j.vibspec.2012.01.019

interface exhibits SPR in the wide angular range, which allows highly accurate computation of the gold film dielectric permittivity.

We assumed a Drude-like expression for the complex dielectric permittivity of gold [25]:

$$\varepsilon = \varepsilon_{\text{Drude}} + \varepsilon_b = 1 - \frac{\omega_p^2\tau^2}{1+\omega^2\tau^2} + i\frac{\omega_p^2\tau}{\omega(1+\omega^2\tau^2)} + \varepsilon'_b + i\cdot\varepsilon''_b \quad (8)$$

where ω_p is the plasma frequency, τ is the relaxation time, ε'_b and ε''_b are the bound electrons' contribution. The experimental spectra from the ZnS/Au/water interface (Eq. (6)) were fitted using Eq. (7). The fitting parameters were ω_p, τ, ε'_b, ε''_b, film thickness d (the same values for all angles), and the incident beam misalignment, $\delta\theta$. The fitting procedure minimizes the following sum:

$$S_1 = \sum_{\nu}(F_{\text{exp}}(\nu,\theta) - F_{\text{model}}(\nu,\theta))^2 \cdot w(\nu,\theta) \quad (9)$$

where weight function $w(\nu,\theta)$ emphasizes the spectral region where the SPR minimum occurs and excludes the regions of strong atmospheric absorption: water vapour absorption at 3100–3850 cm^{-1} and below 2100 cm^{-1}, CO_2 absorption at 2280–2390 cm^{-1}.

4.4. Complex refractive index of dielectric

After determining the dielectric permittivity of the gold film we proceeded to the evaluation of the complex refractive index of the analyte, $n_d + i\kappa_d$. This was done by minimizing the sum:

$$S_2 = \sum_{\theta}(F_{\text{exp}}(\nu,\theta) - F_{\text{model}}(\nu,\theta))^2 w(\nu,\theta) \quad (10)$$

when the model reflectivity F_{model} is described by Eq. (7) with the parameters of the gold film obtained in Section 4.3. Contrary to the previous step, where we fitted the *wave number* dependence of the reflectivity at a fixed angle, here we fitted the *angular* dependence of the reflectivity at each wave number.

5. Results

5.1. Characterization of thin gold film

The experimental setup described in Section 3.1 was used for acquisition of the SPR spectra with cells and water at various angles (see Fig. 3). The position and shape of the SPR spectra with water were utilized for evaluation of thin gold film parameters, namely thickness and complex dielectric permittivity. As described in Section 4.3, we minimized the sum S_1 (Eq. (9)) for 2300–10,000 cm^{-1} spectral region and for five incident angles that exhibit most prominent SPR minimum: $\theta = 13^\circ$, 16°, 24°, 27°, 29°. This yielded parameters of the gold film ω_p, τ, ε_b, and d. Fig. 3 shows that the result of the fitting procedure agrees with the measurements fairly well. We found $\omega_p = 1.32\times10^{16}$ s^{-1}, $\tau = 6.23\times10^{-15}$ s, $\varepsilon'_b = 9.57$, $\varepsilon''_b = 2.51$, $d = 11.6$ nm, and $\delta\theta$ was less than 0.8°. The plasma frequency for our gold thin film is 11% higher than that of the bulk, while the relaxation time is ~36% lower, and this is consistent with the ellipsometric measurements on thin gold films [25,33,35]. The actual film thickness is within 3% from the nominal one estimated by the thickness deposition monitor that is within its precision.

5.2. Complex refractive index of MDCK living cells

Using gold film parameters and the SPR spectra of the prism/gold/MDCK cell monolayer, we determined the complex refractive index of the cells in broad spectral region, as described in Section 4.4. Representative curves of measured and fitted reflectivity versus angle are shown in Fig. 4. The circles present SPR measurements with the prism/gold/MDCK cells trilayer, and the solid line indicates the result of the fitting procedure based on Eq. (10). The fitting procedure works fairly well in the whole spectral region; two examples are shown in Fig. 4: (a) for $\nu = 5088$ cm^{-1}, and (b) for $\nu = 2812$ cm^{-1}. The SPR for the cells is shifted to the lower angle with respect to that of water since the refractive index of cells is higher. Panel (b) of Fig. 5 shows the real and imaginary parts of the refractive index of the cells. The real part of the refractive index of the cells, n_{cell}, exceeds that of the water by 0.025–0.03, depending on the wavelength. The imaginary part of the cells' refractive index mimics the absorption spectrum of water below 4000 cm^{-1}, while above 4000 cm^{-1} the κ_{cell} is mostly featureless and strongly exceeds water absorption due to scattering.

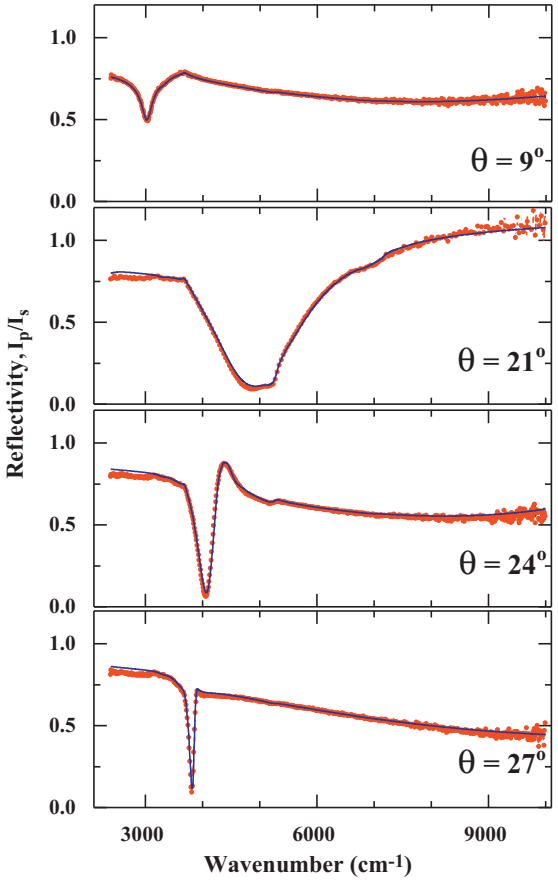

Fig. 3. Measured reflectivity in the SPR regime from the of prism/gold/water trilayer for four different external angles: 9°, 21°, 24°, and 27° (circles). Thickness of gold film is 12 nm. Temperature is 37°C. Solid lines show the model prediction based on Fresnel reflectivity from the prism/gold/water multilayer.

Sensitivity of our method is high enough to discern infrared absorption peaks associated with the organic substances in cells. Fig. 6 shows the scaled absorption spectrum, $\Delta\kappa_{\text{cell}}$, and the derivative of the refractive index $dn_{\text{cell}}/d\nu$ in the 2700–3150 cm^{-1} spectral region. For better presentation, the water absorption is taken as baseline and has been subtracted from the cells' absorption: $\Delta\kappa_{\text{cell}} = \kappa_{\text{cell}} - A\cdot\kappa_{\text{water}}$, where $A < 1$ is constant. The absorption peaks at 2853, 2915, 2954, 3005 and 3039 cm^{-1} correspond to vibrational levels of CH_n (aliphatic) bonds, which are present in various types of biomolecules, but most often in cell membrane lipids [4,5,12,13]. Although real and imaginary parts of the refractive index are evaluated in a fitting procedure independently, each absorption peak has its corresponding feature in the $dn_{\text{cell}}/d\nu$ plot. In this sense, the combination of absorption and refraction

Please cite this article in press as: A. Zilbershtein, et al., Quantitative surface plasmon spectroscopy: Determination of the infrared optical constants of living cells, Vib. Spectrosc. (2012), doi:10.1016/j.vibspec.2012.01.019

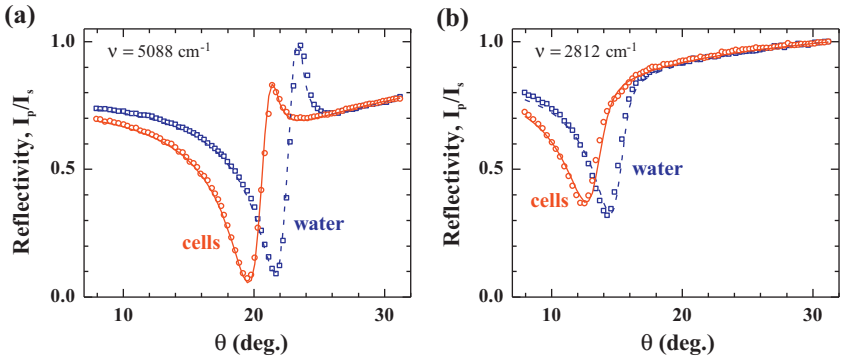

Fig. 4. Measured angular-dependent reflectivity from the prism/gold/MDCK living cells covered with growth medium (circles) and from the prism/gold/water (squares) for two wave numbers: (a) $\nu = 5088\,cm^{-1}$, (b) $\nu = 2812\,cm^{-1}$. Thickness of gold film is 12 nm. Temperature is 37°C. Solid (for cells) and dashed (for water) lines show the model prediction based on known gold film parameters. The fitting procedure yields: (a) $n_{water} = 1.303$, $\kappa_{water} = 1.7 \times 10^{-3}$, $n_{cell} = 1.329$, $\kappa_{cell} = 3.9 \times 10^{-3}$, and (b) $n_{water} = 1.387$, $\kappa_{water} = 6.3 \times 10^{-3}$, $n_{cell} = 1.410$ and $\kappa_{cell} = 9.4 \times 10^{-3}$. The SPR for cells is shifted to lower angle with respect to that of water since the refractive index of cells is higher.

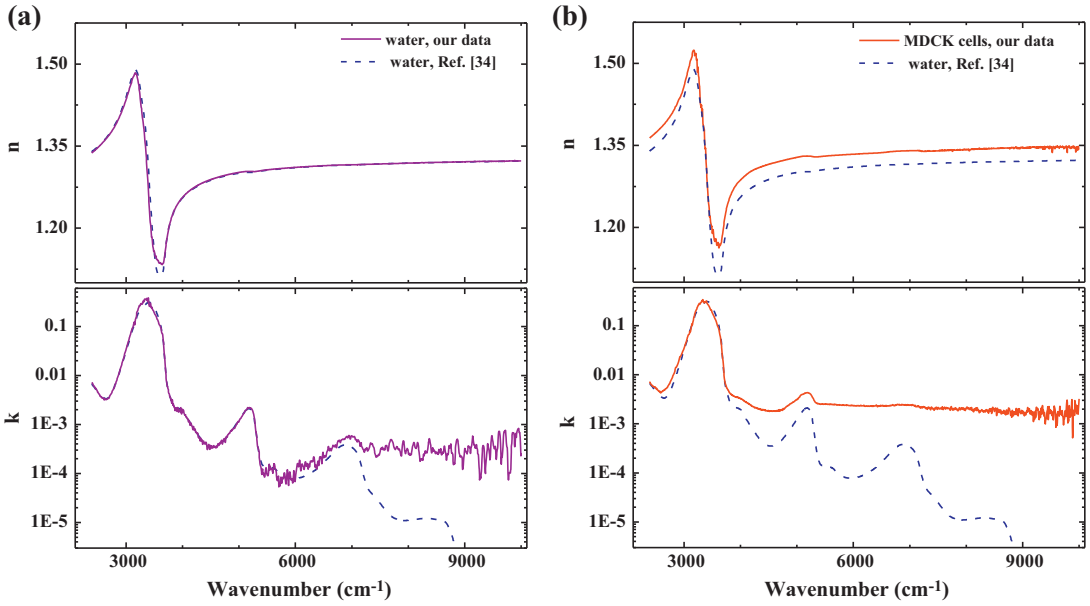

Fig. 5. Real and imaginary parts of refractive index of (a) water, (b) cells, as inferred from our SPR reflectivity measurements (solid lines). The dashed lines in both panels stand for the optical constants of water known from the literature [34].

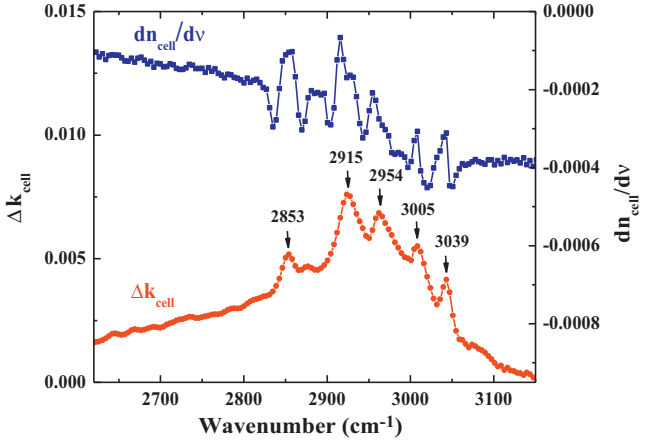

Fig. 6. Imaginary part of the refractive index of MDCK cells in the 2700–3150 cm^{-1} spectral region corresponding to the absorption lines of CH_n bonds (circles). For better visibility the κ plot is baseline corrected. The squares show the derivative of the refractive index. Note absorption peaks at 2853, 2915, 2954, 3005 and 3039 cm^{-1}, which correspond to absorption lines of CH_n bonds, coincide with corresponding features in the $dn_{cell}/d\nu$ curve.

spectroscopy allows pinpointing the vibrational levels with higher accuracy.

6. Discussion

We demonstrate the FTIR-SPR spectroscopy method which is based on the fitting of the experimental SPR spectra to the optical model. Our technique determines with high precision the absolute complex refractive index of the analyte in the broad wavelength region, contrary to previous SPR studies [17–25]. In order to do broadband SPR spectroscopy, we performed measurements for a variety of incident angles. This angular scanning allows us to "cover" the whole spectral region by overlapping SPR curves at different incident angles. However, to make a narrow-band SPR spectroscopy there is no need for such angular scanning although the incident angle should correspond to this particular spectral region.

Our technique does not yield information about single cell; rather it gives information about the population of the cells. The measured intensity of reflected light is the signal from the area containing ~10^5 cells [20], therefore the optical constants measured by our method are averaged over big population of the cells.

Please cite this article in press as: A. Zilbershtein, et al., Quantitative surface plasmon spectroscopy: Determination of the infrared optical constants of living cells, Vib. Spectrosc. (2012), doi:10.1016/j.vibspec.2012.01.019

According to optical microscopy observations, MDCK cells make a fully confluent monolayer on the gold surface.

In order to check the stability of the numerical optical model and find its accuracy, we recalculated water optical constants (Eq. (10)) by using the same SPR spectra from the prism/gold/water interface and gold parameters obtained in Section 5.1. Fig. 4 shows two examples of this calculation. Squares indicate SPR measurements for the prism/gold/water trilayer, and the dashed line shows the fitting curve. Panel (a) of the Fig. 5 shows a good agreement between the complex refractive index of water found from our fitting procedure and the adopted ones [34]. The difference in the real part of the refractive index, n_{water}, is very small (less than 0.001 RIU) except for the 3200–3700 cm^{-1} spectral region. This is the region of strong water absorption where the surface plasmon resonance is severely broadened and barely seen; hence, the fitting procedure is unstable. The difference between the measured and adopted value of the imaginary part of the refractive index, κ_{water}, does not exceed ±5% (up to 10^{-4}) in the 2400–5000 cm^{-1} wavelength region. In the spectral region above 5500 cm^{-1} the sensitivity of the SPR is not enough to measure weak water absorption, because thickness of our gold film is not optimal in this region [17,18,25]. The optimal film thickness depends on wavelength, in particular for gold/water interface it decreases from $d_{opt} \sim 40$ nm at $\nu \sim 10{,}000$ cm^{-1} to $d_{opt} \sim 6$ nm at $\nu \sim 2000$ cm^{-1}. In other words, it is impossible to build a broadband SPR sensor with one gold film thickness. To perform broadband spectroscopy, one can use several sensors with different gold film thicknesses in order to get the highest sensitivity. In this work, we used 12 nm, 15 nm and 20 nm thick gold films that are the most appropriate for the 2400–5000 cm^{-1} spectral region.

We performed three sets of measurements with different prisms and cell layers obtained from the same cell culture. The differences in the optical constants of the cells found in different experiments were of the order of the precision listed above.

6.1. Refractive index of cells

The spectrum of the cell refractive index (real part) mimics that of the water because ~70% of the cell mass is water (see Fig. 5(b), upper panel). However, n_{cell} exceeds that of water, since mineral and organic content of the cells has a higher refractive index [36]. The difference between refractive indices of cells and water, $\Delta n_{cell} = n_{cell} - n_{water}$, decreases monotonically from $\Delta n_{cell} = 0.029$ at $\nu \sim 4000$ cm^{-1} to $\Delta n_{cell} = 0.025$ at $\nu \sim 10{,}000$ cm^{-1}. The explanation for this is related to the way the SP senses the ambient medium. As explained previously, the SP measures the effective refractive index of the dielectric medium, n_{eff}, in the layer of thickness δ_z, which strongly depends on the wavelength (see Eqs. (3–4)). Hence, at different wavelengths the SP senses layers of different thicknesses; particularly at $\nu = 10000$ cm^{-1} it senses a ~0.3 μm thick layer, and at $\nu = 4000$ cm^{-1} it senses a ~2 μm thick layer [17]. The cells' height in our experiments is ~8 μm, as estimated on the base of the guided mode resonance supported by the cell monolayer [17]. The penetration depth of SP is small enough relative to the cells' height in our spectral region, making the contribution of the growth medium above the cells to the effective refractive index, n_{eff}, approximately $\sim 10^{-3}$ RIU, which is within our precision of n_{cell}. Cells and cellular material are inhomogeneous on a micrometer scale in terms of physical morphology and chemical content. Therefore, the effective refractive index at different wavelengths is composed from contributions of different parts of the cell. For instance, the weight of the closest to the gold cell layer (thickness of ~0.1 μm) to the effective refractive index is less than 5% at $\nu = 4000$ cm^{-1} and almost 30% at $\nu = 10000$ cm^{-1}. The optical density of various parts of the cell is different: the cytoplasm is relatively sparse ($n \approx 1.35$, in visible) whereas the nucleus is more optically dense ($n \approx 1.50$, in visible) [36–40]. Since the nucleus is distant from the bottom of the cell (and therefore from the gold film), the surface plasmon at $\nu = 10{,}000$ cm^{-1} does not likely sense the nucleus. Another reason is that the bottom layer of the cell attached to the substrate is not smooth, but has many small protrusions (filopodia) and the gaps between them is filled with the growth medium, whose refractive index is lower than that of cytoplasm ($n \approx 1.34$, in visible) [41,42]. This very thin layer (~0.1 μm) almost does not affect the effective refractive index of the cells at $\nu = 4000$ cm^{-1} but it does affect n_{cell} at $\nu = 10{,}000$ cm^{-1}. All this makes the difference between refractive indices of cells and water, Δn_{cell}, to be lower at $\nu = 10{,}000$ cm^{-1} than at $\nu = 4000$ cm^{-1}.

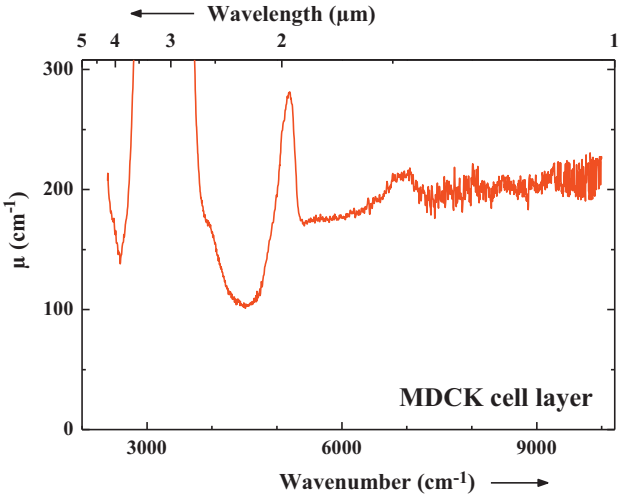

Fig. 7. Attenuation per unit length μ of the surface plasmon wave in MDCK living cell monolayer. μ is dominated by absorption in the spectral region below 5500 cm^{-1} and by scattering in the spectral region above 5500 cm^{-1}.

6.2. Losses: absorption vs scattering

Cells and some subcellular components are of the same size as the probing IR wavelength, which results in large scattering [38–40,43–45]. The imaginary part of the SP wave vector k''_{sp} includes both the absorption and scattering contributions: $k''_{sp} = k''_{abs} + k''_{sca}$. The absorption term reveals specific molecular spectroscopic information that in principle allows the tracing of different cell constituents, such as proteins, lipids, polysaccharides, etc. [1–16], whereas the scattering term is determined by the inhomogeneity of the cells and cell morphology. The lossy part of the cell refractive index, κ_{cell}, is dominated by strong water absorption up to $\nu = 3800$ cm^{-1}, and by scattering in the region above 3800 cm^{-1} (see Fig. 5(b), low panel). Although scattering of the SP waves can be used in cell studies, the lack of adequate theoretical models has prevented the acquisition of quantitative information. Indeed, the SP wave scattering by subwavelength defects [46] or by large objects [47] has been intensively studied, and to the best of our knowledge, the scattering by low-contrast and wavelength size objects such as a confluent layer of cells on the substrate ($r \sim \lambda$, $\Delta n/n < 0.03$) has not been studied theoretically so far. To make comparison with other measurements [48], we calculated the attenuation constant, $\mu = 4\pi\kappa/\lambda$ (see Fig. 7). As can be seen from this plot, the attenuation constant, μ, in the near infrared region (above 5500 cm^{-1}) is about 200 cm^{-1}, which exceeds by several times the attenuation constants for different types of cells measured by the conventional transmission technique. The reason for such a difference is the fact that the surface plasmon is a surface wave and is scattered stronger than the 3D plane wave.

When someone is interested in information about chemical infrared absorbance, there is a need to remove the contribution of

Please cite this article in press as: A. Zilbershtein, et al., Quantitative surface plasmon spectroscopy: Determination of the infrared optical constants of living cells, Vib. Spectrosc. (2012), doi:10.1016/j.vibspec.2012.01.019

scattering from the total attenuation. There are several techniques for doing this, such as extended multiplicative signal correction [44], or performing measurements with plasmonic metal mesh [45]. Our technique offers another possibility: information about chemical absorption might be obtained by differentiation of the real part of the refractive index (see Fig. 6). In the 2700–3150 cm^{-1} spectral region the scattering is weak and losses are dominated by molecular absorption, hence peaks on the $\Delta\kappa_{cell}$ plot are associated with absorption lines only. As might be seen from this plot, these absorption lines coincide with peaks on the plot of the derivative of the real part of the refractive index, $dn_{cell}/d\nu$.

7. Conclusions

We demonstrated the FTIR-SPR technique for spectroscopic study of live MDCK cells in their natural aqueous environment. We measured the complex refractive index of the cells in the spectral region from 2400 cm^{-1} to 10,000 cm^{-1}. Our technique measures the absolute value of the cells' refractive index, n_{cell}, with 10^{-3} RIU accuracy in the majority of the spectral region. The imaginary part of the refractive index, κ_{cell}, can be estimated with an accuracy of 10^{-4}. κ_{cell} contains information about absorption and scattering as well. Our technique offers a straightforward way to get information on absorption lines with very high sensitivity by differentiation of real part of the refractive index n_{cell} with respect to wavelength. We showed the ability of our technique to distinguish absorption lines of specific chemical components of the cells, such as membrane lipids. Our approach has a very good potential for studies, which follow after distribution of different cell components in real time.

Acknowledgements

We are grateful to V. Freilikher for discussions of surface plasmon scattering in cell layers. This research was supported by Israeli Ministry of Industry and Trade through the Nofar program. V. Lirtsman gratefully acknowledges financial support from the Lady Davis Fellowship foundation.

References

[1] D.L. Wetzel, S.M. LeVine, Science 285 (1999) 1224–1225.
[2] G. Hastings, R. Wang, P. Krug, D. Katz, J. Hilliard, Biopolymers 89 (2008) 921–930.
[3] N. Jamin, P. Dumas, J. Moncuit, W.H. Fridman, J.L. Teillaud, G.L. Carr, G.P. Williams, Proceedings of the National Academy of Sciences of the United States of America 95 (1998) 4837–4840.
[4] L.M. Miller, P. Dumas, Biochimica Et Biophysica Acta: Biomembranes 1758 (2006) 846–857.
[5] P. Lasch, M. Boese, A. Pacifico, M. Diem, Vibrational Spectroscopy 28 (2002) 147–157.
[6] H.N. Holman, M.C. Martin, E.A. Blakely, K. Bjornstad, W.R. McKinney, Biopolymers 57 (2000) 329–335.
[7] R. Yamaguchi, A. Hirano-Iwata, Y. Kimura, M. Niwano, K. Miyamoto, H. Isoda, H. Miyazaki, Journal of Applied Physics 105 (2009) 024701.
[8] U. Zelig, J. Kapelushnik, R. Moreh, S. Mordechai, I. Nathan, Biophysical Journal 97 (2009) 2107–2114.
[9] V. Erahimovitch, M. Talyshinsky, Y. Souprun, M. Huleihel, Vibrational Spectroscopy 40 (2006) 40–46.
[10] J. Kneipp, M. Beekes, P. Lasch, D. Naumann, Journal of Neuroscience 22 (2002) 2989–2997.
[11] M.K. Kuimova, K.L.A. Chan, S.G. Kazarian, Applied Spectroscopy 63 (2009) 164–171.
[12] S.M. LeVine, J.D. Radel, J.A. Sweat, D.L. Wetzel, Biochimica Et Biophysica Acta: General Subjects 1473 (1999) 409–417.
[13] F. Draux, P. Jeannesson, C. Gobinet, J. Sule-Suso, J. Pijanka, C. Sandt, P. Dumas, M. Manfait, G.D. Sockalingum, Analytical and Bioanalytical Chemistry 395 (2009) 2293–2301.
[14] N. Jamin, L. Miller, J. Moncuit, W.H. Fridman, P. Dumas, J.L. Teillaud, Biopolymers 72 (2003) 366–373.
[15] R.T. Yamaguchi, A. Hirano-Iwata, Y. Kimura, M. Niwano, K.I. Miyamoto, H. Isoda, H. Miyazaki, Applied Physics Letters 91 (2007) 203902.
[16] M. Romeo, C. Matthaus, M. Miljkovic, M. Diem, Biopolymers 74 (2004) 168–171.
[17] M. Golosovsky, V. Lirtsman, V. Yashunsky, D. Davidov, B. Aroeti, Journal of Applied Physics 105 (2009) 102036.
[18] V. Lirtsman, M. Golosovsky, D. Davidov, Journal of Applied Physics 103 (2008) 014702.
[19] V. Lirtsman, R. Ziblat, M. Golosovsky, D. Davidov, R. Pogreb, V. Sacks-Granek, J. Rishpon, Journal of Applied Physics 98 (2005) 093506.
[20] V. Yashunsky, V. Lirtsman, M. Golosovsky, D. Davidov, B. Aroeti, Biophysical Journal 99 (2010) 4028–4036.
[21] V. Yashunsky, S. Shimron, V. Lirtsman, A.M. Weiss, N. Melamed-Book, M. Golosovsky, D. Davidov, B. Aroeti, Biophysical Journal 97 (2009) 1003–1012.
[22] R. Ziblat, V. Lirtsman, D. Davidov, B. Aroeti, Biophysical Journal 90 (2006) 2592–2599.
[23] A. Ikehata, T. Itoh, Y. Ozaki, Analytical Chemistry 76 (2004) 6461–6469.
[24] H. Kano, S. Kawata, Applied Optics 33 (1994) 5166–5170.
[25] K. Johansen, H. Arwin, I. Lundstrom, B. Liedberg, Review of Scientific Instruments 71 (2000) 3530–3538.
[26] H. Raether, Surface Plasmons on Smooth and Rough Surfaces and on Gratings, Springer-Verlag, Berlin/New York, 1988.
[27] Z. Salamon, H.A. Macleod, G. Tollin, Biochimica Et Biophysica Acta: Reviews on Biomembranes 1331 (1997) 117–129.
[28] Y.C. Chang, R.S. Moirangthem, S.H. Hsu, P.K. Wei, Biosensors & Bioelectronics 25 (2010) 2633–2638.
[29] Materials data from Crystran Ltd., in.
[30] F. Bisio, M. Palombo, M. Prato, O. Cavalleri, E. Barborini, S. Vinati, M. Franchi, L. Mattera, M. Canepa, Physical Review B 80 (2009) 205428.
[31] M. Buskuhl, E.H. Korte, Analytical and Bioanalytical Chemistry 374 (2002) 672–675.
[32] A.I. Maaroof, M.B. Cortie, G.B. Smith, Journal of Optics A: Pure and Applied Optics 7 (2005) 303–309.
[33] A. Nabok, A. Tsargorodskaya, Suryajaya, Physics of Solid State 5 (2008) 1150–1155.
[34] J.E. Bertie, Z.D. Lan, Applied Spectroscopy 50 (1996) 1047–1057.
[35] E.D. Palik, Handbook of Optical Constants of Solids, Academic Press, London, UK, 1985.
[36] F.P. Bolin, L.E. Preuss, R.C. Taylor, R.J. Ference, Applied Optics 28 (1989) 2297–2303.
[37] X.J. Liang, A.Q. Liu, C.S. Lim, T.C. Ayi, P.H. Yap, Sensors and Actuators A: Physical 133 (2007) 349–354.
[38] B. Mohlenhoff, M. Romeo, M. Diem, B.R. Woody, Biophysical Journal 88 (2005) 3635–3640.
[39] M. Romeo, M. Diem, Vibrational Spectroscopy 38 (2005) 129–132.
[40] M. Romeo, B. Mohlenhoff, M. Diem, Vibrational Spectroscopy 42 (2006) 9–14.
[41] C.L. Curl, C.J. Bellair, T. Harris, B.E. Allman, P.J. Harris, A.G. Stewart, A. Roberts, K.A. Nugent, L.M.D. Delbridge, Cytometry Part A 65A (2005) 88–92.
[42] J.J. Ramsden, R. Horvath, Journal of Receptors and Signal Transduction 29 (2009) 211–223.
[43] P. Bassan, H.J. Byrne, J. Lee, F. Bonnier, C. Clarke, P. Dumas, E. Gazi, M.D. Brown, N.W. Clarke, P. Gardner, Analyst 134 (2009) 1171–1175.
[44] A. Kohler, J. Sule-Suso, G.D. Sockalingum, M. Tobin, F. Bahrami, Y. Yang, J. Pijanka, P. Dumas, M. Cotte, D.G. van Pittius, G. Parkes, H. Martens, Applied Spectroscopy 62 (2008) 259–266.
[45] M.A. Malone, S. Prakash, J.M. Heer, L.D. Corwin, K.E. Cilwa, J.V. Coe, Journal of Chemical Physics 133 (2010) 185101.
[46] F. Pincemin, A.A. Maradudin, A.D. Boardman, J.J. Greffet, Physical Review B 50 (1994) 15261–15275.
[47] D.C. Prieve, J.Y. Walz, Applied Optics 32 (1993) 1629–1641.
[48] W.F. Cheong, S.A. Prahl, A.J. Welch, IEEE Journal of Quantum Electronics 26 (1990) 2166–2185.

Please cite this article in press as: A. Zilbershtein, et al., Quantitative surface plasmon spectroscopy: Determination of the infrared optical constants of living cells, Vib. Spectrosc. (2012), doi:10.1016/j.vibspec.2012.01.019